Audible Noise and Corona Discharge from Water Droplets on Superhydrophobic HVAC Conductors

Xu Zhang, Ian Cotton*, *Senior Member*, *IEEE*, Simon Rowland, *Fellow, IEEE*, Qi Li, *Member, IEEE*, Chengxing Lian, Wenyuan Li and Chorphaka Plaengpraphan

Abstract—**Audible noise from transmission lines is mainly generated by corona discharge from defects and water droplets on the conductors' surface. Applying a superhydrophobic coating to the conductors can reduce corona discharge, thereby reducing the level of audible noise produced. In this paper, corona discharge and noise measurements from an untreated conductor and a conductor coated with superhydrophobic coatings were carried out in AC electric fields and continuous water spray. The coated conductors show higher partial discharge inception voltages (PDIV) than uncoated ones. PD magnitude and PD per cycle of the coated conductors are lower compared with uncoated conductors, especially at electric fields above 14 kV/cm. A linear correlation between overall sound pressure and total PD magnitude is established. The behavior of corona discharges from single droplets with various sizes and positions and associated droplet vibration were investigated and the local electric field enhancement was analyzed by finite element analysis to examine the influence of droplet size and position on electric field distribution. Superhydrophobic coatings result in reduced PD magnitude and number and therefore reduce audible noise generated. This is attributed to small sessile droplets forming rather than large pendant droplets.**

Index Terms- **overhead line conductors, audible noise, corona discharge, superhydrophobic coatings, water droplets.**

I. INTRODUCTION

ULTRA-HIGH voltage (UHV) and Extra-high voltage (EHV) transmission lines have been increasingly used to meet the growing demand for electrical transmission capacity [1]–[3]. Though overhead line conductors are readily designed to fulfill the electrical and mechanical requirements, corona discharge can be induced by protrusions introduced by extrinsic factors such as pollution, water droplets, surface defects and ice on the conductor surface. These features can, due to the resulting elevated local electric field, result in corona loss, audible noise and radio interference [4]–[6]. Therefore, a number of environmental factors including the maximum electric field and audible noise levels need to be considered for overhead line conductor design [7]–[10].

Corona discharge occurs with the local electric field exceeding an inception field and will result in corona loss and acoustic noise [11]. The influence of the average surface roughness on the corona inception voltage and the audible noise under the dry condition has been investigated [12] [13]. Due to the higher surface roughness developed over time, conductors which have been in service longer have a lower corona discharge onset voltage than newer conductors and thus show higher audible noise levels at the same voltage in dry conditions. The surface discharge on the polluted surface is more likely to propagate in the air while its propagation path is mainly along the clean surface [14] [15]. Teich compared the corona current characteristics of conductors with various surfaces – untreated, hydrophobic and highly hydrophilic surfaces under continuous rain [16]. It was found that the water spread uniformly on the highly hydrophilic conductor while pendant and sessile droplets formed on the other two conductors' surfaces. Correspondingly, the corona current generated from the droplets of the highly hydrophilic conductor was the least. Xu [5] examined the dynamic characteristics of AC corona discharge under conditions of rain. Discharges on the upper and lower surfaces had different characteristics but both occurred in the positive cycle of the voltage waveform. Taylor cone discharge formed in the negative cycle of the voltage waveform with relatively stable droplet oscillations on the conductor [5]. Furthermore, Miyajima explored the influence of the conductor surface condition (from hydrophilic to superhydrophobic) and found that superhydrophobic surfaces might help reduce the noise levels by minimizing the presence of droplets on the conductor [17].

Typically, noise measurements are not carried out in an anechoic chamber, and so background noise, for example from supply transformers, is not eliminated. Therefore, a semi-anechoic chamber in the high voltage lab of the University of Manchester was built to reduce baseline noise levels. A comparison of untreated conductors and conductors with a superhydrophobic coating under a continuous water spray and an AC voltage was then carried out and reported in our previous paper [18]. It was shown that the $2f$ hum noise and overall sound pressure levels can both be reduced with a superhydrophobic coating. A comparison of the droplet distributions gave some evidence for the cause of noise reduction [18].

Xu Zhang is with the School of Engineering, University of Warwick, Coventry, CV4 7AL, UK. (email: Xu.Zhang.1@warwick.ac.uk)

Ian Cotton, Simon Rowland, Qi Li, Wenyuan Li and Chorphaka Plaengpraphan are with the School of Engineering, The University of Manchester, Manchester, M13 9PL, UK.
(email: ian.cotton@manchester.ac.uk; s.rowland@manchester.ac.uk; qi.li@manchester.ac.uk, wenyuan.li-2@postgrad.manchester.ac.uk; chorphaka.plaengpraphan@postgrad.manchester.ac.uk)

Chengxing Lian is with the School of Engineering, Imperial College London, London, SW7 2BX, UK. (email: c.lian22@imperial.ac.uk).

The durability and reliability of superhydrophobic surfaces are essential to their application in power transmission systems. Our previous work compared the aging performance of a silicone-based superhydrophobic coating and microscale structured surface after thermal cycling, outdoor aging and corona discharge exposure [19]. The two superhydrophobic surfaces both maintained superhydrophobicity after thermal cycling and outdoor aging but were degraded after corona exposure. Another nano-composite superhydrophobic coating was exposed to corona discharge generated by a needle electrode and results show that the coating would be aged but could recover under low-intensity corona discharge [20]. However, the corona discharge in these two aging experiments was generated by a high-voltage needle which is likely to be more severe than in operational conditions. Therefore, various techniques have been developed to create robust superhydrophobic surfaces. The combination of micro-structure and nano-structure to form a superhydrophobic surface was reported recently [21] [22]. The microstructure was used to protect the nanostructure which provides superhydrophobicity, which can maintain a high contact angle (above 150°) after abrasion and scratch tests [21]. Furthermore, a self-healing superhydrophobic surface was created by integrating anodization with the infusion of a healing agent fluoroalkylsilane [23]. The superhydrophobicity can be restored by the healing agent when heated at 70 °C for a duration of 30 minutes [23]. Such work on developing robust superhydrophobic surfaces is required to support their application in practice.

The literature shows that droplets are the main reason for audible noise generation on HV conductors. The relationship between the noise level and rainfall rate and electric field has been examined, but the influence of the size and position of water droplets on the audible noise and corona discharge have not been investigated in any detail. This paper aims to correlate noise reduction due to a superhydrophobic coating on a conductor with corona discharge characteristics and changes in droplets' size and position.

II. EXPERIMENTAL METHODOLOGY

A. Samples

Test samples were traditional Aluminum Conductor Steel Reinforced conductors and Gap-Type High-Temperature Low Sag conductors, with diameters of 31.6 mm and lengths of 4 m, as shown in Fig. 1. These are referred to as ACSR and GAP, respectively. The ACSR comprises round strands of 3.53 mm diameter, and the GAP conductor has strands with a flattened external surface.

A commercial superhydrophobic coating, NeverWet® produced by Rust-Oleum, was evenly applied to some of the conductors to achieve superhydrophobic surfaces. While this coating would unlikely be used in a commercial application as it would likely age rapidly, it provides a simple way of manufacturing samples in a repeatable manner for the test within the HV laboratory environment. Before the application of the coating, the samples were cleaned in an ultrasonic acetone bath at 25°C for 10 mins. Subsequently, the samples were rinsed in deionized water, immersed in isopropanol, and
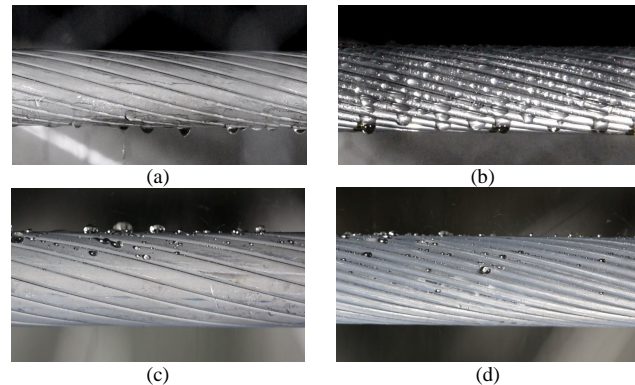

Fig. 1. The water droplets distribution without applied voltage on: (a) uncoated GAP, (b) uncoated ACSR, (c) coated GAP and (d) coated ACSR.[18]

left to dry at room temperature overnight. The NeverWet® coating containing three layers was sprayed onto the conductor, with the detailed procedure given in our previous paper [18], to achieve superhydrophobicity. The base layer mainly comprises aliphatic hydrocarbons, which can generate microstructures on surfaces. The key constituents of the top layer consist of acetone, propane, n-Butane, and silicone. Silicone particles are incorporated to fill the gaps between the microstructures of the base layer, thereby enhancing the superhydrophobic characteristics.

Due to the difficulty of quantifying the static contact angles on the curved surfaces of conductors, a flat aluminum alloy 6082 substrate (a typical overhead line conductor material) was used to assess the superhydrophobicity of the coating, using a DataPhysics OCA 15EC goniometer. The average contact angle of the coated sample was 162.4° (above 150° is recognized as superhydrophobic) while uncoated samples gave an average contact angle of 85.3°. The droplet distribution around the conductor circumference was heavily affected by the superhydrophobic coating, which was discussed in [18] as shown in Fig. 1. The water droplets are mainly distributed on the bottom surface of the uncoated GAP and are spread all around the uncoated ACSR. For coated conductors, fewer and smaller water droplets are mostly retained on the top of the conductors, and the downward-facing surfaces tend to be dry.
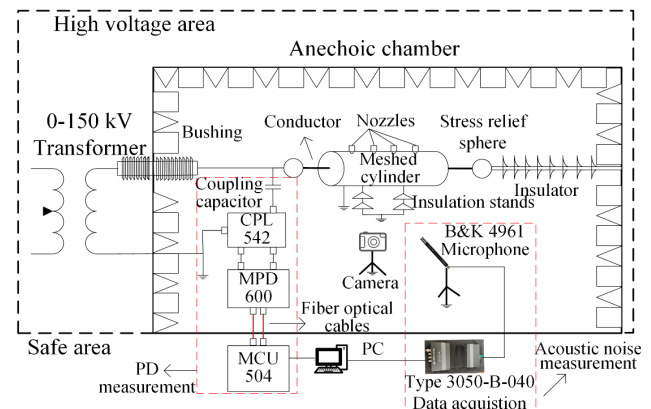

Fig. 2. Schematic of an experimental setup. The sample under test is 4 m long.

B. High voltage experimental setup

The high voltage experimental setup is shown in Fig. 2. A semi-anechoic chamber with dimensions of 10.5×4.3×3.0 m was built in the lab to minimize the background noise from the outer room and the 50 Hz HV transformer. More detail is given in our previous paper [18]. The inner walls of the anechoic chamber have wedges attached, which are filled with porous foam to reduce sound reflection. A 150 kV transformer was external to the chamber and connected to the conductor with a bushing. An earthed mesh cage with a diameter of 150 cm was placed around the conductor to achieve the design conductor surface electric field at a relatively low voltage level and ensure the electric field was circumferentially uniform [18]. The surface electric field in this test ranges from 6 kV/cm to 21 kV/cm (rms) and is calculated based on the perfect model of cylinders (i.e. without strands) shown in the following equation [24].

$$E = \frac{U}{r * \ln(R/r)} \tag{1}$$

where R is the radius of the earthed cage, U is the applied voltage, E is the equivalent electric field and r is the radius of the conductor. The typical surface gradient for a 400 kV transmission system is around 18 kV/cm (rms) [25]. Spheres at the end of the conductors are used to manage the fields and avoid localized discharges.

A Brüel & Kjær Type 4961 multi-field microphone was placed at the same height as the conductor to measure noise levels. The LAN-XI Data acquisition hardware (Type 3050-B-040), shown in the red square on the right of Fig. 2, connects the microphone and the computer over an ethernet cable. The acoustic analysis software PULSE Labshop is used to record and analyze the noise waveform. To measure and analyze the high-frequency electrical signals generated by the partial discharge (PD) events on the conductors, an Omicron MPD Partial Discharge Analysis system was utilized, as illustrated in the red square on the left of Fig. 2. A coupling capacitor (1 nF) was connected in series between the test conductor and the measuring system, including measuring impedance CPL 542 and an MPD 600 unit. Then MCU 504 control unit is connected to the MPD 600 unit through fiber optical cable to minimize ground loops and reduce interference coupling. The camera was used to observe the droplet distribution on the conductors. The adjustable nozzles were connected to a regulator to spray tap water at a rate of 20 mm/h, which meets the wet test standard in IEC 60060-1 [26].

III. RESULTS AND ANALYSIS

A. Partial discharge characteristics

Typical phase-resolved partial discharge (PRPD) patterns measured when testing uncoated and coated conductors are shown in Fig. 3. PD events mainly occur during the rising part of the positive and negative cycles of voltage. For a typical corona discharge PRPD pattern, small relatively constant magnitude but repetitive pulses occur in the negative half cycle adjoining the peak voltage and fewer but larger pulses exist in the positive half cycle [27] [28]. The reason for the
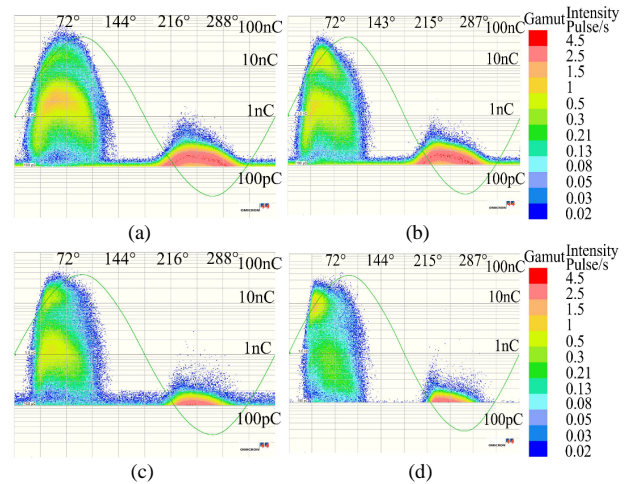

Fig. 3. PRPD pattern of conductors at 20 mm/h for: (a) uncoated GAP, (b) uncoated ACSR, (c) coated GAP and (d) coated ACSR. The color bar is the same for all plots.

corona discharge PRPD pattern is due to the difference in the mechanism between negative and positive corona discharge. In the case of negative corona discharge, the electrons are generated by the electrode and subsequently drift away from the ionizing region and move into the drifting region with the lower potential gradient. On the other hand, the positive corona discharge is initiated by an external ionization event occurring in a high potential gradient region and the generated electrons are attracted toward the electrode, resulting in a lower density of electrons compared with the negative corona discharge. Therefore, the electrons during positive discharge can gain higher energy and lead to higher discharge magnitude and the lower electron density results in a lower discharge frequency than the negative corona discharge [11]. PRPD patterns shown in Fig. 3 have a phase shift, which may be the results of the asynchrony of water drop vibration with different sizes and voltage waveform.

The partial discharge inception voltage (PDIV) and partial discharge extinction voltage (PDEV) were measured three times for each conductor in the rain condition. The corresponding electric fields were calculated by equation (1) and the average values are summarized in Table I. The PDIV of uncoated conductors is around 37 kV, lower than PDIV of coated conductors. According to our previous results, the discharges mainly exist at the tip of the water droplets [18]. The distribution of droplets shown in Fig. 1 varies between uncoated and coated conductors, with large pendant droplets

TABLE I
The PDIV and PDEV and corresponding surface electric fields for uncoated and coated conductors

	Uncoated GAP	Coated GAP	Uncoated ACSR	Coated ACSR
PDIV(kV)	37.07	46.06	36.76	47.08
PD inception field(kV/cm)	6.08	7.55	6.03	7.72
PDEV(kV)	33.62	43.04	33.61	44.28
PD extinction field(kV/cm)	5.51	7.06	5.51	7.26

This article has been accepted for publication in IEEE Transactions on Power Delivery. This is the author's version which has not been fully edited and content may change prior to final publication. Citation information: DOI 10.1109/TPWRD.2023.3293869
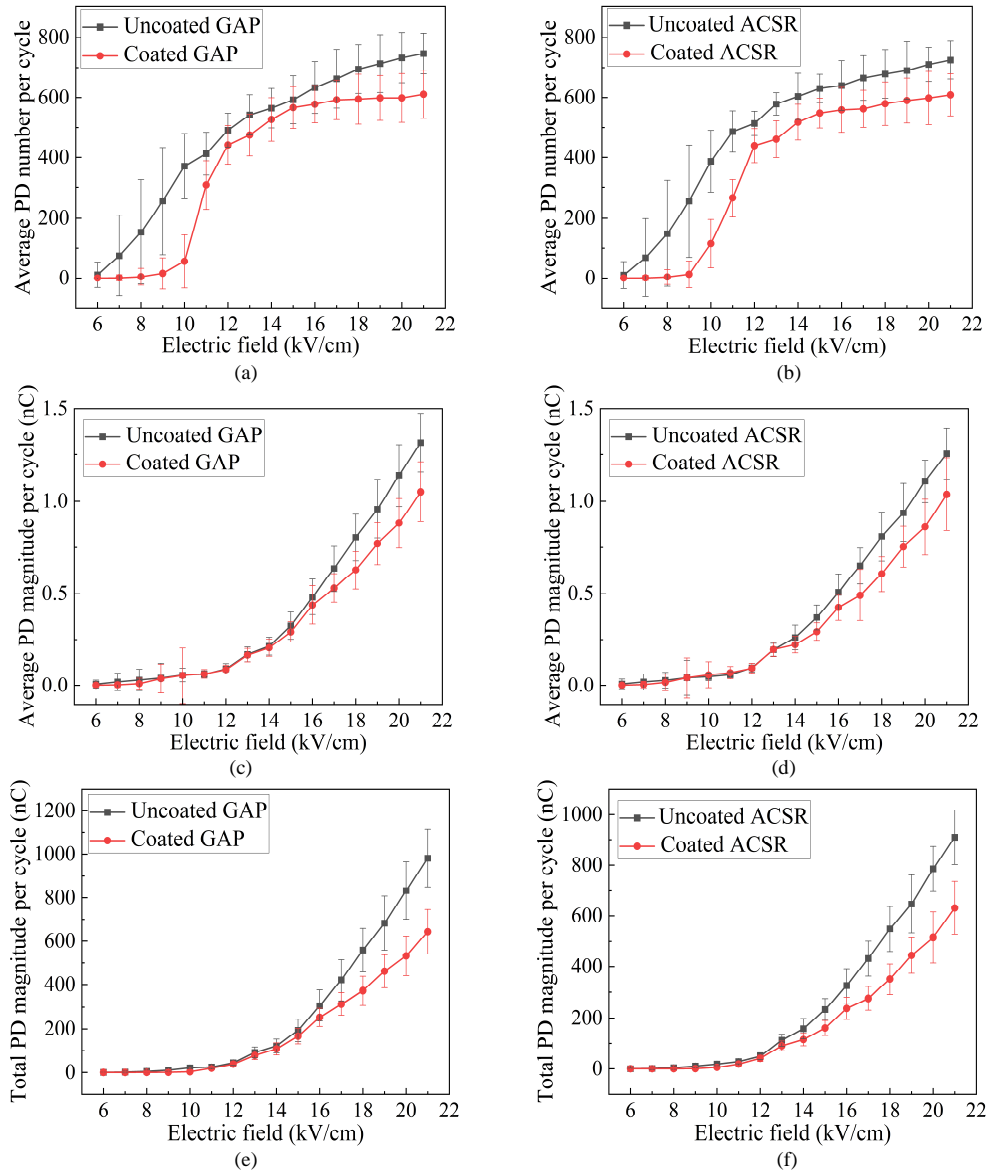
4

Fig. 4. The PD parameters for uncoated and coated conductors. (a) and (b) are average PD number per cycle; (c) and (d) are average PD magnitude per cycle; (e) and (f) are total PD magnitude per cycle. The error bars represent the standard deviation of the PD parameters for each field.

being dominant on uncoated conductors, while small sessile droplets mainly exist on coated conductors. The average size of water droplets on uncoated conductors is larger than that of coated conductors, which may account for the lower PDIV for uncoated samples. The position of water droplets on the uncoated and coated conductor also likely affects the PDIV. The impact of the droplet size and position on PD performance is discussed in detail in Section C.

PD events were measured for one minute at each electric field. The parameters extracted from the PD events data, including the average PD magnitude per cycle, average PD number per cycle, and the total PD magnitude per cycle (the PD number multiplied by the average PD magnitude in one cycle), are shown in Fig. 4. The PD magnitude represents the amplitude of each individual PD event, while the PD number represents the frequency of PD events. As shown in Fig. 3, while negative discharges are responsible for determining the PD number, positive discharges make a greater contribution to the overall magnitude of PD, which likely indicates the

severity of corona discharge [11]. The PD parameters show similar trends for GAP and ACSR conductors. Coated conductors have a lower average PD number per cycle for all electric fields, probably due to the fewer droplets on the coated surfaces. Below 11 kV/cm, there are few PD for the coated conductors. As fields are increased above 11 kV/cm, there is a rapid increase in discharges on the coated conductors but the number remains lower than for uncoated ones.

The ejection phenomenon (small water droplet emission) from sessile droplets on the coated conductor was found at 11 kV/cm [18], which may cause an increasing PD number. However, the pendant droplet on the uncoated conductor can eject small droplets in a lower electric field (7 kV/cm), resulting in a higher PD number than that for the coated conductor. There is no obvious difference between the uncoated and coated conductors in average PD magnitude per cycle, when the electric field is below 14 kV/cm. The coated conductors have a lower average PD magnitude when the

electric field is above 14 kV/cm, and the highest reduction occurs at the highest electric field. The total PD magnitude has a similar behavior to the average PD magnitude. Overall, the superhydrophobic coating will result in higher PDIV, lower PD number and lower PD magnitude, especially above 14 kV/cm.

B. Correlation between PD performance and audible noise

The unweighted overall sound pressure level (SPL), shown in Fig. 5, was relatively constant for uncoated and coated conductors below 14 kV/cm. The SPL increases with the electric field at around 1.25 dB/kV/cm and 1 dB/kV/cm for uncoated GAP and ACSR respectively, but the coated conductors show a reduced noise level (by a maximum of 3.46 dB and 2.19 dB for coated GAP and ACSR respectively) compared to uncoated above 14 kV/cm, indicating a correlation with PD performance shown in Fig. 4.

There is a strong positive linear relationship between the overall SPL and the total PD magnitude per cycle as shown in Fig. 6. The coefficient of determination ($R^2 > 0.96$) confirms the strong fitness of the linear parameters for GAP and ACSR conductors. The gradients from Fig. 6 are close to each other, in the range of 0.012-0.015 dB/nC.

As described in the introduction, the audible noise contains low-frequency and high-frequency components. Therefore, the correlation between partial discharge behavior and sound
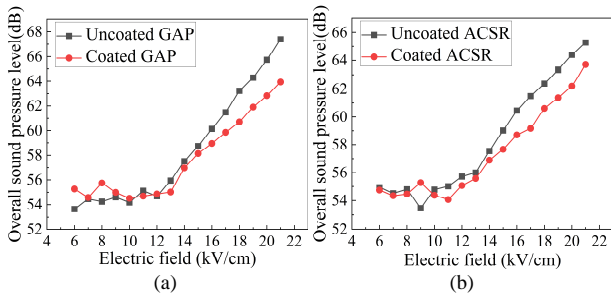

Fig. 5. Overall sound pressure level of uncoated and coated conductors. (a) GAP conductors, (b) ACSR conductors.
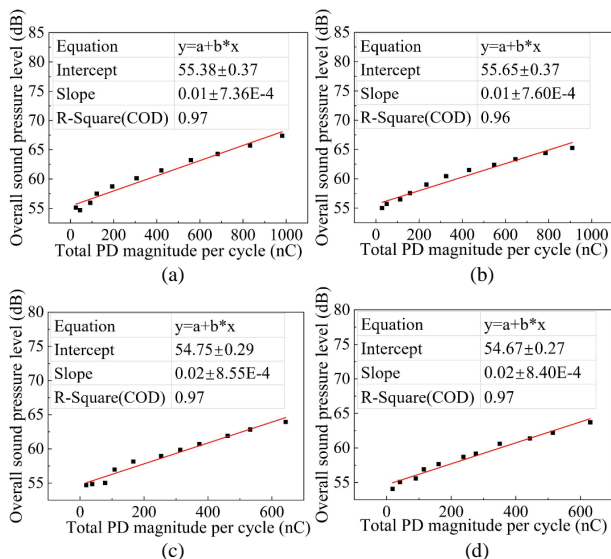

Fig. 6. The correlation of overall sound pressure level the total PD magnitude per cycle of uncoated and coated conductors. (a) uncoated GAP, (b) uncoated ACSR, (c) coated GAP and (d) coated ACSR.
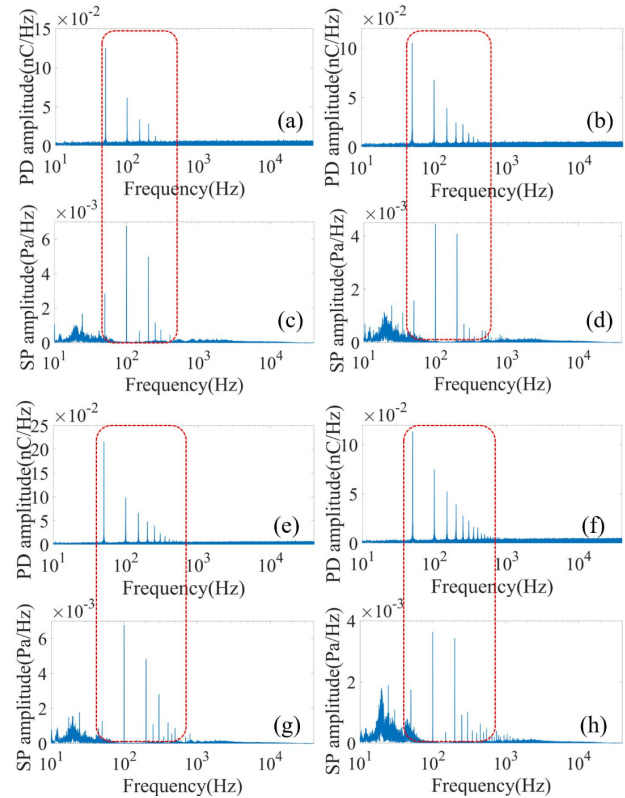

Fig. 7. The frequency spectrum of the sound pressure (SP) and the PD magnitude at 18 kV/cm. (a) and (c) are uncoated GAP, (b) and (d) are coated GAP, (e) and (g) are uncoated ACSR, (f) and (h) are coated ACSR.

pressure in the frequency domain needs careful examination. The PD events measured over time by the Omicron MPD system were subjected to a Fast Fourier Transform (FFT) to obtain the PD amplitude in the frequency domain. The sound pressure (SP) in the frequency domain was also derived with FFT and summarized in Fig. 7. The data shown in Fig. 7 is based on the surface electric field of 18 kV/cm (rms) because it is equivalent to the average field strength seen on a 400 kV (rms) system twin bundle RUBUS conductor [29].

It can be seen in Fig. 7 that several peaks of PD amplitude and sound pressure amplitude were found in the frequency domain, ranging from 50 Hz to 600 Hz (red square) for both uncoated and coated conductors. This shows a correlation of PD and acoustic noise in the low-frequency domain. The electrical breakdown of the air around the droplets caused by corona discharge can result in high-frequency crackling noise [30]. However, few PD amplitude and sound pressure amplitude peaks were found in the high-frequency domain. In our previous paper, it was found that low-frequency noise is more dominant in the frequency spectrum compared with high-frequency noise [18].

According to Li [31], the peak at 50 Hz is mostly due to the modulation of AC voltage. More PD amplitude and sound pressure amplitude peaks are found for coated conductors than with uncoated conductors in Fig. 7. In the rain condition, at least two types of discharge exist on the normal conductors including discharges when droplets hit the conductor and discharges from the tip of deforming droplets [5]. For the
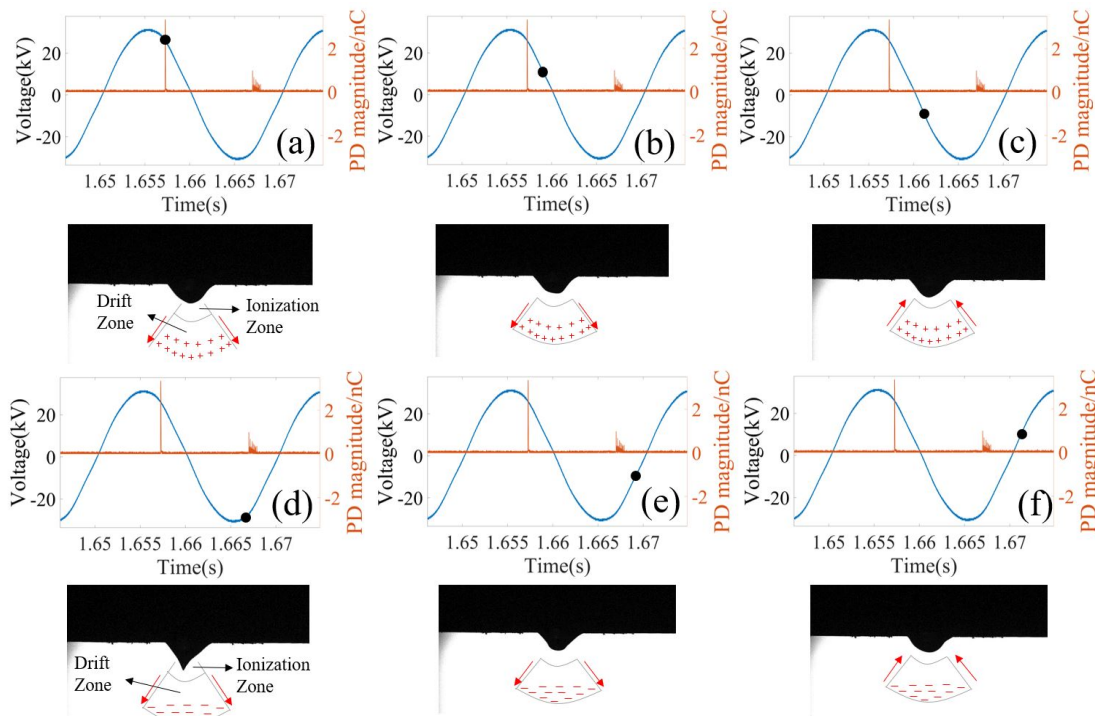
Fig. 8. A model for the movement of ions during synchronous pendant water vibration and corona discharge behavior in an AC voltage cycle; the red arrow represents the ions' movement direction.

coated conductors, the droplet gains charge on contact with the conductor by contact electrification [32]. Then another source of discharge is found between the charged droplet and the conductor when it bounces off the coated conductor. This is not seen on uncoated conductors. This may be the cause of more peaks in the frequency spectrum.

To understand the relationship between noise generation and discharge behavior, the voltage waveform, PD events and single pendant droplet vibration are synchronously shown in Fig. 8. It was achieved by employing a pulse generator to generate a pulse to trigger simultaneously the high-speed camera and oscilloscope which was connected to a PD test kit. In addition, the potential role of space charge is illustrated in Fig. 8. In one voltage cycle, there is one large positive discharge and several negative discharges with a low magnitude, similar to the PD behavior under continuous water spraying. The higher magnitude discharges on the positive cycle with a frequency of 50 Hz may also reflect the PD amplitude peak at 50 Hz in Fig. 7. The positive discharge is not seen at the highest voltage because the drop vibration lags the voltage variation. At the falling part of the positive voltage waveform, the positive corona discharge occurs when the drop is pointed or cone-like, as shown in Fig. 8 (a). At this time molecules in the air are ionized, generating electrons and positive ions in the ionization zone around the conductor. The electrons are attracted toward the conductor electrode, and the positive ions are repelled and accelerated in the drift zone in the direction of the electric field. The collisions between the positive ions and neutral molecules will generate sound pressure pulses [33], [34]. When the voltage is below the discharge extinction voltage, there is no discharge activity.

The positive ions continue to drift away from the conductor. Then the voltage is changed in polarity but not enough to trigger negative discharge. The positive ions are attracted by the conductor in the negative voltage cycle, as shown in Fig 8 (c). As the voltage rises, the negative corona discharge occurs with the Taylor cone [35]. The electrons generated by ionization move outwards from the conductor and attach oxygen molecules to form negative ions, which will be accelerated in the drift zone and then move towards the conductor when the voltage changes to positive. Therefore, in one AC voltage cycle, the ions are attracted and repelled twice the frequency of the voltage frequency, which is the reason for the generation of sound pressure at 100 Hz. The other low-frequency noise peaks are mainly the harmonics corresponding with the partial discharge peaks [31].

Therefore, the superhydrophobic surfaces can be potentially applied to the conductor to reduce the audible noise and corona discharge because of their positive linear correlation described above. It is also feasible to employ this correlation to detect and monitor the corona discharge by acoustic detection which is a non-direct contact and non-intrusive technique [36] [37].

C. Influence of droplet size and position on PD

With the superhydrophobic coating applied on the conductors, the fewer and smaller sessile droplets become dominant on the coated conductors compared with the larger and more pendant droplets prevalent on the uncoated conductors, as shown in Fig. 1. The previous sections of this paper illustrate the correlation between noise performance with corona discharge behavior under the continuous water spraying. Thus, this section will investigate the discharge

TABLE II
The PDIV and PD magnitude and number of droplets with various sizes and positions

	PDIV (kV)	Average PD magnitude per cycle (nC)	Average PD number per cycle
0.01ml pendant droplet	28.80	5.07	37.79
0.01ml sessile droplet	30.10	2.32	6.63
0.03ml sessile droplet	28.20	4.43	51.59

behavior of single pendant and sessile droplets with various sizes to correlate the noise reduction with corona discharge.

Single pendant and sessile droplets with volumes of 0.01 ml or 0.03 ml were chosen to examine the influence of the droplet position on the discharge behavior. The volume of water droplets was calculated from the diameter and height of the droplet cones on the conductors, measured by image software (ImageJ). The minimum and maximum droplet volume is 0.005 ml and 0.03 ml. We chose 0.01 ml and 0.03 ml droplets as a typical example to investigate the size effect on discharge activity. Each single droplet was placed on an uncoated GAP conductor with a length of 10 cm within an
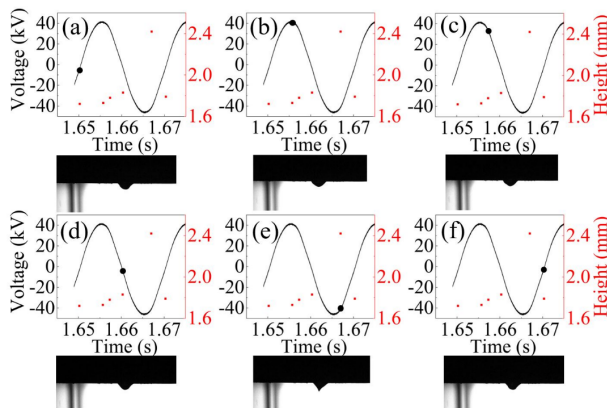

Fig. 9. The 0.01 ml pendant drop vibration and corresponding voltage. The red points represent the highest height of the drop at that voltage. The axes of all plots are the same.

Fig. 10. The 0.01 ml sessile drop vibration and corresponding voltage. The red points represent the highest height of the drop at that voltage. The axes of all plots are the same.
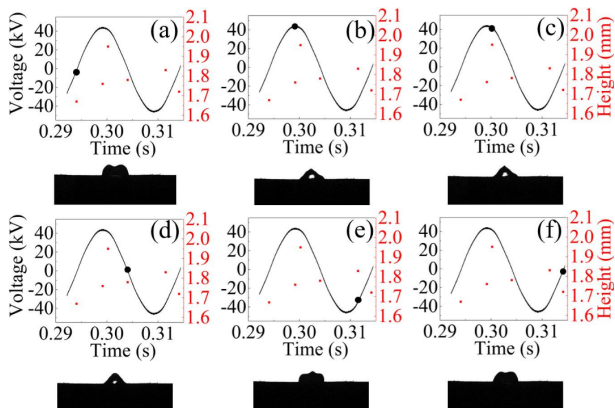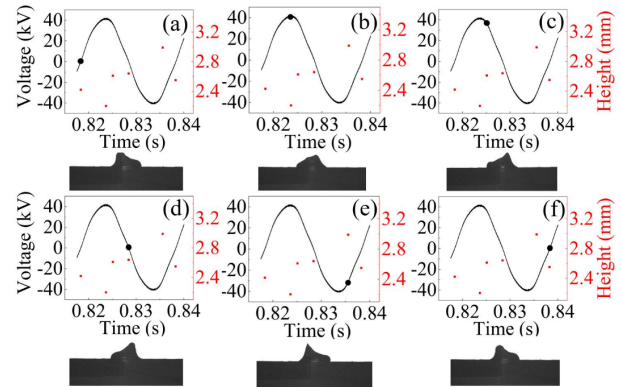

Fig. 11. The 0.03 ml sessile drop vibration and corresponding voltage. The red points represent the highest height of the drop at that voltage. The axes of all plots are the same.

earthed cylindrical cage of 5 cm radius to study its partial discharge behavior.

The PDIV, PD magnitude and number per cycle for each case are summarized in Table II. It is shown that the PDIV of the sessile drop is higher than the pendant drop of the same size, which corresponds to the higher PDIV of coated conductors shown in Table I. Furthermore, the average PD magnitude and PD number per cycle of the sessile droplet are lower than that of the pendant droplet, partly explaining the lower PD magnitude and PD number for coated conductors with continuous rain. The smaller sessile droplet shows a higher PDIV and lower PD magnitude and number than the larger one. Therefore, the droplet distribution and size both influence the discharge behavior.

The partial discharge is strongly related to the droplet's oscillation and the corresponding voltage and frequency. We note there will be a difference in droplet response under 50 Hz and 60 Hz, so the power frequency does matter in this case [15]. The vibration of the 0.01 ml pendant and sessile drop corresponding with the AC voltage is shown in Fig. 9 and Fig. 10. Meanwhile, the greatest height during the droplet vibration is also plotted with the red points representing the droplet deformation. The sessile drop shows the highest height of 1.95 mm in the positive cycle, while it is 2.42 mm for the pendant droplet in the negative cycle. The ratio of the highest and lowest height can be used to describe the deformation degree. It is 1.41 for the pendant droplet and 1.17 for the sessile droplet, calculated from Fig. 9 and Fig. 10, also showing more severe deformation of the pendant droplet. The pendant drop will be elongated more than the sessile drop with the same size in one voltage cycle. In terms of the size effect, a 0.03 ml sessile droplet has a lower PDIV and higher PD magnitude and PD number than a 0.01 ml sessile droplet, as shown in Table II. The droplet vibrates in two directions in one voltage cycle and shows different vibration modes with others, which may relate to the size of the droplet and contact angle and surface conditions [15], [40]. The highest height during the whole cycle is 2.99 mm and the highest and lowest height ratio is 1.36, higher than that of a 0.01 ml sessile droplet.

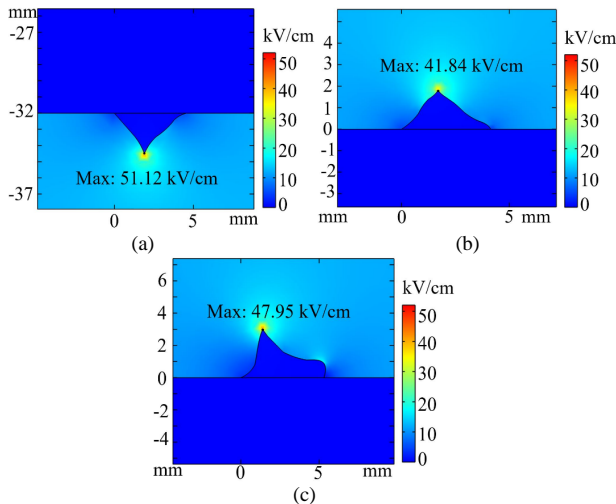To investigate the local electric field enhancement around

Fig. 12. The local electric field distribution around droplets on the conductor. (a) 0.01 ml pendant droplet, (b) 0.01 ml sessile droplet and (c) 0.03 ml sessile droplet.

the droplet, 2D Finite Element Analysis (FEA) models of the most severe droplet deformations in Fig. 9 - Fig. 11 were built in COMSOL. These are shown in Fig. 12. The simulation results show that the highest electric fields exist at the tip of the droplet. This was also seen in [39]–[41]. The maximum electric field around a 0.01 ml sessile droplet is lower than for a 0.01 ml pendant droplet and a 0.03 ml sessile droplet, corresponding to the droplet deformation degree. The higher local electric field can also result in a lower PDIV and higher PD magnitude and number.

Overall, the PD behavior related to the single droplet vibration process shows that small sessile droplets lead to higher PDIV, lower PD magnitude and lower PD number compared to the large pendant droplet, which explains the weaker corona discharge of coated conductor, thus resulting in the noise reduction with superhydrophobic coating.

IV. DISCUSSION

The PD behavior under continuous water spraying shows that the total PD magnitude of the coated conductors is lower than the uncoated conductors, resulting in lower audible noise, especially when the electric field is above 14 kV/cm as shown in Fig. 4 (c)-(f). The ejection phenomenon was found to take place around 11 kV/cm [18]. The water droplet starts to vibrate and eject smaller drops from the main droplet, likely generating more discharge events. As the electric field continues to rise, the volume of droplets is reduced due to the continuous ejection process. However, there is no stable Taylor cone formed at this electric field. At lower fields then, no obvious PD magnitude reduction is found on coated conductors. At 14 kV/cm, a dynamic balance of the droplet ejection and water accumulation under the continuous rain was established to form a relatively stable Taylor cone, as shown in Fig. 13. The volumes and the positions of the droplets are almost constant from 14 kV/cm for each case studied. Therefore, the PD magnitude shows a reduction for coated conductors because of the fewer and smaller droplets on the coated surfaces. Relative PD magnitude reduction

decreases more significantly with the rising electric field. The statistical droplet distributions on uncoated and coated conductors presented in our previous paper showed that the mean droplet diameters on coated GAP and ACSR conductors were decreased by 47.8 % and 12.8 % respectively compared with uncoated conductors [18].

The corona discharge activity corresponds with the droplet vibration process and so relates to the droplet size. Hu built a pendant water droplet deformation model based on the shape change under the alternating electric force and gravity to investigate the influence of droplet size on corona inception voltage [42]. The results show that the highest height of pendant droplets increases, and the corona inception voltage decreases with the larger droplet radius. For the sessile droplets studied in this paper, larger droplets exhibit different vibration modes with a higher degree of deformation than small droplets, resulting in lower PDIV, as shown in Table II. According to the modeling in Fig. 12, larger droplets have a higher local electric field around the droplet tip and are therefore more prone to induce corona discharges than smaller droplets.

The deformation degree of droplets is dependent on the droplet resonant frequency and the electric field frequency. When the two frequencies are close, the vibration amplitude of droplets will be large [5]. Fujii [43] studied the vibration behavior of uncharged and charged water droplets under a 50 Hz electric field and concluded that the vibration frequency of uncharged droplets is 100 Hz while it is 50 Hz for charged water droplets. The charged water droplets will be under the electric force (Coulomb's force) under the AC electric field, which is expressed as

$$f = qE \propto qE \sin \omega t \qquad (2)$$

where q is the amount of charge.

Therefore, the vibration frequency of charged water droplets in the corona discharge situation will be the same as the applied voltage frequency (50 Hz), as shown in Fig. 9-Fig. 11. According to [38] [44], the natural vibration
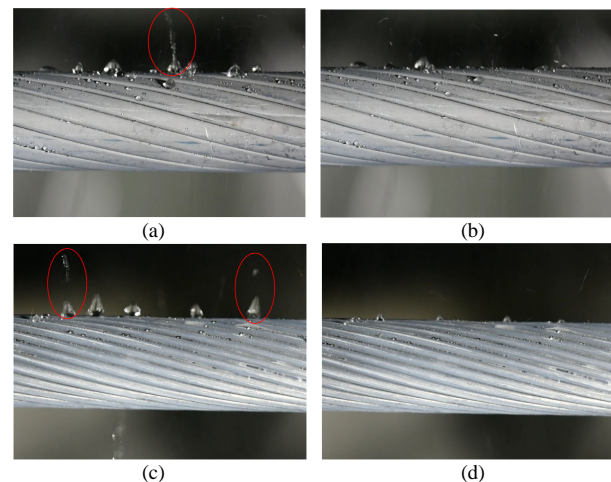

Fig. 13. The droplets distribution on coated conductors at different electric fields. (a) is coated GAP under 11 kV/cm [18], (b) is coated GAP under 14 kV/cm, (c) is coated ACSR under 11 kV/cm [18] and (d) is coated ACSR under 14 kV/cm. (a) and (c) illustrate droplet emission.

frequency, f_0, of water droplets can be expressed as

$$f_0 = \frac{\alpha\pi}{2}\left(\frac{n^3\gamma}{24\rho V} \cdot \frac{(\cos^3\theta - 3\cos\theta + 2)}{\theta^3}\right)^{\frac{1}{2}} \quad (3)$$

where γ is the coefficient of the surface tension (0.073 N m^{-1} at 20°C); ρ and V are the density and volume of the droplet, respectively; n represents the number of oscillation modes of the droplet (3 and 4 for 0.01 ml and 0.03 ml sessile droplets respectively [45]); α is a constant of order unity (0.81)[45], and θ is the contact angle of uncoated surface which is 85.3°.

According to equation (3), the natural angular frequency of 0.01 ml and 0.03 ml sessile droplets are 84 Hz and 75 Hz. Thus, the angular frequency of the bigger sessile droplet is closer to the applied electric field frequency, resulting in a larger deformation degree. Qi compared the vibration magnitude (the tip of the droplet to the base of the electrode) of sessile water droplets with various sizes ranging from 2 µl to 8 µl under 50 Hz AC electric field and found that the bigger droplet has the larger vibration magnitude [41]. It was also found that the bigger droplets have a lower nature angular frequency [5]. The pendant droplets have a higher vibration amplitude due to their physical nature and gravity compared with the sessile droplets. Therefore, the change from large pendant droplets to small sessile droplets due to applied superhydrophobic coatings may drive the audible noise reduction with the lower PD number and PD magnitude.

In addition to reducing corona discharge and audible noise, as described in this and our previous paper [18], the application of superhydrophobic surfaces can also be beneficial to anti-icing, anti-frosting and anti-corrosion for transmission lines [46]. A superhydrophobic aluminum surface was developed by chemical etching to fabricate a hierarchical micro/nanostructure and it can delay the freezing time to 5100 s compared with the ordinary aluminum freezing time (260 s) [47]. The ice adhesion strength can also be reduced from 710 kPa to 45 kPa [48] and the frost formation can be delayed for 140 min on a superhydrophobic conductor surface [49]. In natural conditions, the wind will cause conductor vibrations including aeolian vibrations and galloping vibrations [50]. Wind-induced conductor vibrations can further reduce droplet accumulation on superhydrophobic conductor surfaces, which can contribute to reducing corona discharge, audible noise, ice/frost deposition, and overall improve transmission line performance.

V. Conclusions

Partial discharge behavior of conductors with a standard finish and conductors coated with superhydrophobic coatings under continuous water spraying was measured alongside audible noise emissions under AC voltages. The measured PDIV of coated conductors is higher than uncoated ones. Compared to the uncoated conductors, the coated conductors have a lower average PD number per cycle, PD amplitude per cycle, and total PD amplitude per cycle, which also results in lower audible noise levels, especially when the surface electric field is above 14 kV/cm. A linear correlation between overall sound pressure levels and the total PD magnitude per cycle

was established for uncoated and coated conductors. The PD magnitude peaks are also correlated with sound pressure peaks in the frequency domain. A comparison of the corona discharge behavior corresponding to droplet vibration shows that the PDIV of a single pendant droplet is lower, and the PD number and magnitude per cycle are higher than that of a sessile droplet of the same volume. Large sessile droplets (0.03 ml) have a lower PDIV and higher PD amplitude and number per cycle than small sessile droplets (0.01 ml). These observations explain the lower PD number and magnitude of coated conductors in continuous rain. FEA results show that the local electric field is highest for the small pendant droplet and the lowest for the small sessile droplet. The large sessile droplet generates a higher electric field than the small sessile droplet. Therefore, the droplet size distribution and location changing from large pendant droplets on uncoated conductors to small sessile droplets on coated conductors results in a lower PD number and magnitude.

These observations provide the explanation for the audible noise reduction on conductors with superhydrophobic coatings and give confidence for their application. In addition, in practical applications, there will always be wind or conductor vibration happening on the conductors, which will likely further reduce the accumulation of water droplets on the superhydrophobic conductor and thereby decrease the corona discharge and audible noise.

VI. Acknowledgment

VII. References

[1] H. N. Scherer and G. S. Vassell, "Transmission of electric power at Ultra-High voltages: current status and future prospects," *Proc. IEEE*, vol. 73, no. 8, pp. 1252–1278, Aug. 1985.

[2] Y. Shu and W. Chen, "Research and application of UHV power transmission in China," *High Volt.*, vol. 3, no. 1, pp. 1–13, Mar. 2018.

[3] M. Candas and O. S. Meric, "The application of Ultra High Voltage in the world," *J. Power Energy Eng.*, vol. 03, no. 04, pp. 453–457, Feb. 2015.

[4] Y. Liu, L. Zhou, Y. Liu, H. Yuan, L. Ji, and Q. Wang, "Analysis on the spectrum characteristic of corona Current and its relationship with Radio Interference on UHVDC transmission line," *IEEE Trans. Dielectr. Electr. Insul.*, vol. 23, no. 6, pp. 3336–3345, Dec. 2016.

[5] P. Xu, B. Zhang, Z. Wang, S. Chen, and J. He, "Dynamic characteristics of corona discharge generated under rainfall condition on AC charged conductors," *J. Phys. D. Appl. Phys.*, vol. 50, no. 50, Nov. 2017.

[6] G. W. Juette and L. E. Zaffanella, "Radio noise, audible noise, and corona loss of EHV and UHV transmission lines under rain: Predetermination based on cage tests," *IEEE Trans. Power Appar. Syst.*, vol. PAS-89, no. 6, pp. 1168–1178, Jul. 1970.

[7] J. Pihler and I. Tičar, "Design of systems of covered overhead conductors by means of electric field calculation," *IEEE Trans. Power Deliv.*, vol. 20, no. 2 I, pp. 807–814, Apr. 2005.

[8] B. J. Maddock, "Overhead line design in relation to electric and magnetic field limits," *Power Eng. J.*, vol. 6, no. 5, pp. 217–224, Sep. 1992.

[9] J. Smede, C. G. Johansson, O. Winroth, and H. P. Schat, "Design Of Hvdc Converter Stations With Respect To Audible Noise

This article has been accepted for publication in IEEE Transactions on Power Delivery. This is the author's version which has not been fully edited and content may change prior to final publication. Citation information: DOI 10.1109/TPWRD.2023.3293869

10

Requirements," *IEEE Trans. Power Deliv.*, vol. 10, no. 2, pp. 747–758, Apr. 1995.

[10] B. M. Weedy, "Environmental aspects of route selection for overhead lines in the U.S.A.," *Electr. Power Syst. Res.*, vol. 16, no. 3, pp. 217–226, May. 1989.

[11] X. Li, J. Wang, Y. Li, Q. Zhang, T. Lu, and X. Cui, "Correlation between audible noise and corona current generated by AC corona discharge in time and frequency domains," *Phys. Plasmas*, vol. 25, no. 6, Jun. 2018.

[12] X. Bian, L. Chen, D. Yu, L. Wang, and Z. Guan, "Impact of surface roughness on corona discharge for 30-year operating conductors in 500-kV ac power transmission line," *IEEE Trans. Power Deliv.*, vol. 27, no. 3, pp. 1693–1695, Apr. 2012.

[13] X. Bian *et al.*, "Influence of aged conductor surface conditions on AC corona-generated audible noise with a corona cage," *IEEE Trans. Dielectr. Electr. Insul.*, vol. 19, no. 6, pp. 2037–2043, Dec. 2012.

[14] X. Meng, H. Mei, B. Zhu, F. Yin, and L. Wang, "Influence of pollution on surface streamer discharge," *Electr. Power Syst. Res.*, vol. 212, no. 108638, Jul. 2022.

[15] X. Meng, H. Mei, F. Yin, and L. Wang, "The Development of the streamer discharge to flashover along the dielectric surfaces," *IEEE Trans. Dielectr. Electr. Insul.*, Early access, Mar. 2023.

[16] T. H. Teich and H.-J. Weber, "Origin and abatement of tonal emission from high voltage transmission lines," *e i Elektrotechnik und Informationstechnik*, vol. 119, no. 1, pp. 22–27, Jan. 2002.

[17] K. Miyajima and K. Tanabe, "Evaluation of audible noise from surface processing conductors for AC overhead transmission line," *Electr. Eng. Japan (English Transl. Denki Gakkai Ronbunshi)*, vol. 159, no. 3, pp. 19–25, Mar. 2007.

[18] X. Zhang *et al.*, "Experimental verification of the potential of superhydrophobic surfaces in reducing audible noise on HVAC overhead line conductors," *High Volt.*, vol. 7, no. 4, pp. 692–704, Mar. 2022, doi: 10.1049/hve2.12200.

[19] C. Lian *et al.*, "Assessing the superhydrophobic performance of laser micropatterned aluminium overhead line conductor material," *IEEE Trans. Power Deliv.*, vol. 37, no. 2, pp. 972–979, Apr. 2022.

[20] X. Wang, X. Li, Q. Lei, W. Li, and Y. Wu, "Influence of alternating current (AC) corona discharge on the superhydrophobicity of SiO$_2$/fluorosilicon resin nano-composite coating," *Appl. Surf. Sci.*, vol. 478, pp. 642–650, Jun. 2019.

[21] D. Wang *et al.*, "Design of robust superhydrophobic surfaces," *Nature*, vol. 582, no. 7810, pp. 55–59, Jun. 2020.

[22] G. Wang, S. Liu, S. Wei, Y. Liu, J. Lian, and Q. Jiang, "Robust superhydrophobic surface on Al substrate with durability, corrosion resistance and ice-phobicity," *Sci. Rep.*, vol. 6, pp. 1–10, Feb. 2016.

[23] G. Y. Liu *et al.*, "Robust and self-healing superhydrophobic aluminum surface with excellent anti-icing performance," vol. 28, no. 101588, Feb. 2022.

[24] V. Megala and C. P. Sugumaran, "Effect of Radio Interference in 765kV Zebra Conductor with Different Bundle Configurations," *in Proc. Int. Conf. on Nascent Technologies in Engineering Vashi,* India, 2017, pp. 1-6.

[25] Q. Li, S. M. Rowland, I. Dupere, and R. Shuttleworth, "Acoustic noise evaluation for overhead line conductors using an anechoic chamber," *IEEE Trans. Power Deliv.*, vol. 32, no. 4, pp. 1835–1843, Aug. 2017.

[26] *High voltage testing techniques — Part 1: General definitions and test requirements*, International Standard IEC 60060, 1990.

[27] R. P. Nair and S. B. Vishwanath, "Analysis of partial discharge sources in stator insulation system using variable excitation frequency," *IET Sci. Meas. Technol.*, vol. 13, no. 6, pp. 922–930, Aug. 2019.

[28] M. Wahyudi, "Audiosonic Acoustic Detection of Air Corona Discharge based on Fast Fourier Transform," *Int. Conf. High Volt. Eng. Power Syst.*, 2019, pp. 2–7.

[29] Q. Li, "Acoustic Noise Emitted from Overhead Line Conductors," Ph.D. dissertation, Dept. Elect. Eng., Manchester Univ., Manchester, UK, 2013.

[30] S. Hedtke, L. Zaffanella, M. Pfeiffer, J. Chan, C. M. Franck, and J. Bell, "Audible noise of hybrid AC/DC overhead lines: Comparison of different prediction methods and conductor arrangements," *in Proc. Int. Conf. EPRI HVDC and FACTS*, 2015, pp. 1-9.

[31] X. Li, J. Wang, T. Lu, and X. Cui, "Statistical analysis of audible noise generated by AC corona discharge from single corona

[32] sources," *High Volt.*, vol. 3, no. 3, pp. 207–216, Sep. 2018.

[32] U. G. Musa, S. D. Cezan, B. Baytekin, and H. T. Baytekin, "The Charging Events in Contact-Separation Electrification," *Sci. Rep.*, vol. 8, no. 1, pp. 1–8, Feb. 2018.

[33] U. Straumann, "Mechanism of the tonal emission from ac high voltage overhead transmission lines," *J. Phys. D. Appl. Phys.*, vol. 44, no. 7, Jan. 2011.

[34] U.Straumann;J.Fan, "Tonal Component of the Audible Noise From Uhv-AC Transmission Lines," *2009 Int. Conf. UHV Transm.*, 2009, pp. 1–5.

[35] C. T. R. Wilson and G. I. Taylor, "The bursting of soap-bubbles in a uniform electric field," *Math. Proc. Cambridge Philos. Soc.*, vol. 22, no. 05, p. 728, Oct. 1925.

[36] M. Dong, A. Ma, M. Ren, C. Zhang, J. Xie, and R. Albarracín, "Positioning and imaging detection of corona discharge in air with double helix acoustic sensors array," *Energies*, vol. 10, no. 12, Dec. 2017.

[37] S. Suwanasri *et al.*, "Partial Discharge Investigation and Failure Analysis on Distribution Network Using Acoustic Camera," *Proceeding 2021 9th Int. Electr. Eng. Congr. iEECON, 2021*, pp. 181–184.

[38] R. H. Temperton and J. S. Sharp, "Vibrational modes of elongated sessile liquid droplets," *Langmuir*, vol. 29, no. 15, pp. 4737–4742, Mar. 2013.

[39] M. H. Nazemi and V. Hinrichsen, "Partial Discharge Investigation and Electric Field Analysis of Different Oscillation Modes of Water Droplets on the Surface of Polymeric Insulator under Tangential AC Electric Field Stress," *in Proc. Int. Conf. Solid. Dielectr.*, 2013, pp. 194–197.

[40] Q. Li, R. Shuttleworth, I. Dupere, G. Zhang, and M. Rowland, "FEA modelling of a water droplet vibrating in an electric field," *in Proc. IEEE Int. Symp. Electr, Insul.* 2012, pp. 449–453.

[41] Q. Li, S. M. Rowland, I. Dupere, and R. Morris, "The impact of water droplet vibration on corona inception on conductors under 50 Hz AC fields," *IEEE Trans. Power Deliv.*, vol. 33, no. 5, pp. 2428-2436, Apr. 2018.

[42] Q. Hu *et al.*, "Minimum steady corona inception voltage calculation method under rain condition," *IET Gener. Transm. Distrib.*, vol. 12, no. 8, pp. 1783–1789, Feb. 2018.

[43] O. Fujii, K. Honsali, Y. Mizuno, and K. Naito, "Vibration of a water droplet on a polymeric insulating material subjected to AC voltage stress," *IEEE Trans. Dielectr. Electr. Insul.*, vol. 17, no. 2, pp. 566–571, Apr. 2010.

[44] X. Noblin, A. Buguin, and F. Brochard-Wyart, "Vibrated sessile drops: Transition between pinned and mobile contact line oscillations," *Eur. Phys. J. E*, vol. 14, no. 4, pp. 395–404, Aug. 2004.

[45] R. Temperton, "Resonant Vibrations of Microlitre Liquid Drops," M.S. thesis, Dept. Electr. Eng., Nottingham Univ., Nottingham, UK, 2012.

[46] B. Li *et al.*, "A Review on Superhydrophobic Surface with Anti-Icing Properties in Overhead Transmission Lines," *Coatings*, vol. 13, no. 2, Jan. 2023.

[47] M. Fenero, M. Knez, I. Saric, M. Petravic, and H. Grande, "Omniphobic etched aluminum surfaces with anti-icing ability´," *Langmuir*, vol. 36, no. 37, pp: 10916-10922, Aug. 2020.

[48] Y. Xie *et al.*, "Rational Fabrication of Superhydrophobic Nanocone Surface for Dynamic Water Repellency and Anti-icing Potential," *J Bionic Eng.*, vol. 16, pp. 27–37, Jan. 2019.

[49] Z. Zuo, R. Liao, X. Zhao, X. Song, Z. Qiao, and C. Guo, "Anti-frosting performance of superhydrophobic surface with ZnO nanorods," *Appl. Therm. Eng.*, vol. 110, pp. 39–48, Jan. 2017.

[50] A. Rossi, C. Jubayer, H. Koss, D. Arriaga, and H. Hangan, "Combined effects of wind and atmospheric icing on overhead transmission lines," *J. Wind Eng. Ind. Aerodyn.*, vol. 204, no. 104271, Sep. 2020.

VIII. BIOGRAPHIES

Xu Zhang was born in Henan, China, in 1993. He received the B. S. degree and master's degree in electrical engineering from Xi'an Jiaotong University in 2014 and 2017 respectively, Ph.D. degree from The University of Manchester in 2021. Currently, he is a Research Fellow at The University of Warwick. His main research is on audible noise characteristics of overhead line conductor, superhydrophobic coating material, and insulation material.

Ian Cotton received a Class I B.Eng. (Hons.) degree in electrical engineering from the University of Sheffield, Sheffield, U.K., in 1995 and the Ph.D. degree in electrical engineering from the University of Manchester, Institute of Technology (UMIST), Manchester, U.K., in 1998. He is currently a Professor of High Voltage Technology at the University of Manchester and the Director of Manchester Energy. His main research interests include power systems transients, the use of higher voltage systems in aerospace applications and power system induced corrosion.

Simon M. Rowland (SM '07, F '014) was born in London, England. He completed the B.Sc. degree in physics at The University of East Anglia and the Ph.D. degree at London University. He has worked for many years on dielectrics and their applications and has also been Operations and Technical Director within multinational manufacturing companies. He joined The School of Electrical and Electronic Engineering in The University of Manchester as a Senior Lecturer in 2003, and was appointed Professor of Electrical Materials in 2009, and was Head of School 2015-19. He was President of the IEEE Dielectric and Electrical Insulation Society in 2011 and 2012 and is currently serving as its Treasurer.

Qi Li (aka Steven) was born in Hunan, China, in September 1984. He completed the B.Eng. at both the University of Birmingham and Huazhong University of Science and Technology in 2007, M.Sc. with distinction in Electrical Power Engineering from the University of Manchester in 2009, and Ph.D. in the same institution in 2013. Since then he has been working for the University of Manchester and National Grid UK for 6 years before joining Chongqing University as a '100 Talents Plan Associate Professor' of Chongqing City. Acting as main contributor, he has won twice the IET innovation awards (2012 and 2015). He is an active member in CIGRE working group B2.69, a committee member in IEEE PES Transmission & Distribution Satellite Committee and a youth committee member in China Electrotechnical Society.

Chengxing Lian received a First‑Class B.Eng. (Hons.) degree in Electrical and Electronic Engineering from the University of Manchester, U.K., a First‑Class B.Eng. degree in Electrical Engineering and Automation from North China Electric Power University, China, in 2016 and Ph.D. degree from The University of Manchester in 2021. His main research interests include ageing and performance assessments of superhydrophobic surface treatments on overhead lines.

Wenyuan Li received a B.Eng degree in Electrical Engineering from the University of Liverpool, U.K., in 2016 and an MSc degree in Electrical Power System from the University of Manchester. He is currently working towards his PhD degree in Electrical Engineering at the University of Manchester. His main research interest is creepage distance in aerospace high voltage systems.

Chorphaka Plaengpraphan was born in Bangkok, Thailand. She received the B.Eng. degree in Industrial Electrical Engineering from Thammasat University, Thailand, in 2014, the M.Eng and MSc. degrees in Industrial Electrical Engineering and Electrical Power System Engineering from Thammasat University, Thailand and The University of Manchester, U.K., in 2016 and 2018, respectively. She is now currently a PhD candidate at The University of Manchester. Her research interests include insulator and its performance, HV technology and railway application.